1

Enhancement of Vascular Structures in 3D and 2D Angiographic Images

Tim Jerman, Franjo Pernuš, Boštjan Likar, and Žiga Špiclin

Abstract—A number of imaging techniques are being used for diagnosis and treatment of vascular pathologies like stenoses, aneurysms, embolisms, malformations and remodelings, which may affect a wide range of anatomical sites. For computer-aided detection and highlighting of potential sites of pathology or to improve visualization and segmentation, angiographic images are often enhanced by Hessian based filters. These filters aim to indicate elongated and/or rounded structures by an enhancement function based on Hessian eigenvalues. However, established enhancement functions generally produce a response, which exhibits deficiencies such as poor and non-uniform response for vessels of different sizes and varying contrast, at bifurcations and aneurysms. This may compromise subsequent analysis of the enhanced images. This paper has three important contributions: i) reviews several established enhancement functions and elaborates their deficiencies, ii) proposes a novel enhancement function, which overcomes the deficiencies of the established functions, and iii) quantitatively evaluates and compares the novel and the established enhancement functions on clinical image datasets of the lung, cerebral and fundus vasculatures.

Index Terms—angiography, vascular pathology, vessel, bifurcation, tube-like, enhancement filter, Hessian eigenvalue analysis

I. Introduction

ASCULAR pathologies like stenoses, aneurysms, embolisms, malformations and remodelings may affect a wide range of anatomical sites including cerebral, hepatic, cardiac, pulmonary, peripheral, retinal, etc. The need for early diagnosis and effective treatment of vascular pathologies led to the development of a variety of vascular imaging techniques. Because imaging plays an important role in the diagnosis, treatment and follow-up of vascular pathologies, further improvement of these processes is immediately possible by advancing the acquisition and/or image analysis techniques.

Vascular imaging or angiography involves 2D and 3D acquisition techniques like ophthalmic fundus imaging, contrast enhanced X-ray and digital subtraction angiography (DSA), ultrasound, computed tomography angiography (CTA) and magnetic resonance angiography (MRA). The choice of an optimal imaging modality for a specific anatomical site or vascular pathology may depend on several factors. For instance, because of high resolution on a macroscopic level, DSA is a reference standard for diagnosis of various vascular pathologies, e.g. aneurysms [1], [2]. The DSA is an invasive imaging modality, while CTA and MRA are minimally invasive alternatives, but generally have a lower resolution

The authors are with the University of Ljubljana, Faculty of Electrical Engineering, Tržaška cesta 25, SI-1000 Ljubljana, Slovenia.

E-mail: {tim.jerman, franjo.pernus, bostjan.likar, ziga.spiclin}@fe.uni-lj.si.

compared to DSA [3]. For diagnosing the aneurysms, however, a combined strategy of CTA, MRA and DSA imaging is preferred as it is most cost-effective [4]. Several anatomical sites and vascular pathologies may require imaging modalities different from DSA, CTA and MRA. For instance, diabetic retinopathy is diagnosed by optical coherence tomography or color imaging of the fundus [5]. Because angiographic acquisitions vary substantially in contrast, resolution, noise and artifacts and because vascular networks are often complex and surrounded by other structures, visual inspection of angiographic images, let alone the diagnosis and quantification of vascular pathologies, is clearly a difficult task.

Computer aided systems based on image analysis can reduce the amount of time a clinician spends to inspect an image, but also to diagnose and quantify vascular pathologies more accurately and reliably. Image analysis, for instance, may involve only detection and highlighting of potential sites of pathology [6]-[8] or segmentation and quantification of the vascular structures [9]. However, such analyses are often not robust to highly varying intensities of vascular structures, related to non-uniform contrast distribution across a vascular network during image acquisition. When imaging a (large) vascular network, even an ideally timed contrast bolus may be non-uniformly distributed throughout the network, while within and across vessels, blood flow velocity variations due to laminar flow can disrupt contrast agent distribution and further increase the non-uniformity. To remove to some extent these undesired intensity variations in angiographic images, and to suppress non-vascular structures and image noise, filters for enhancing vascular structures are used extensively.

Among filtering methods for vascular structures, image derivatives are widely used as they encode border (first order derivatives) and shape (second order derivatives) information about the structures in an image. For instance, structure tensors [10]-[12] are based on first order derivatives and used to enhance boundaries of prominent local contrast and direction. Such filters are generally susceptible to the presence of noise in regions of uniform intensity. A large class of filtering methods employs the analysis of Hessian matrix [13]— [17], which is based on second order derivatives and which enables differentiation between rounded, tubular, and planar structures. Alternative to the Hessian matrix is the Weingarten matrix [18], which is a combination of first and second order derivatives. Vessel enhancement diffusion [19] combines Hessian and diffusion filtering to further reduce the impact of background noise. The mentioned filters are all based on Gaussian scale space, hence, they may fuse adjacent vessel boundaries. The boundaries can be preserved by employing

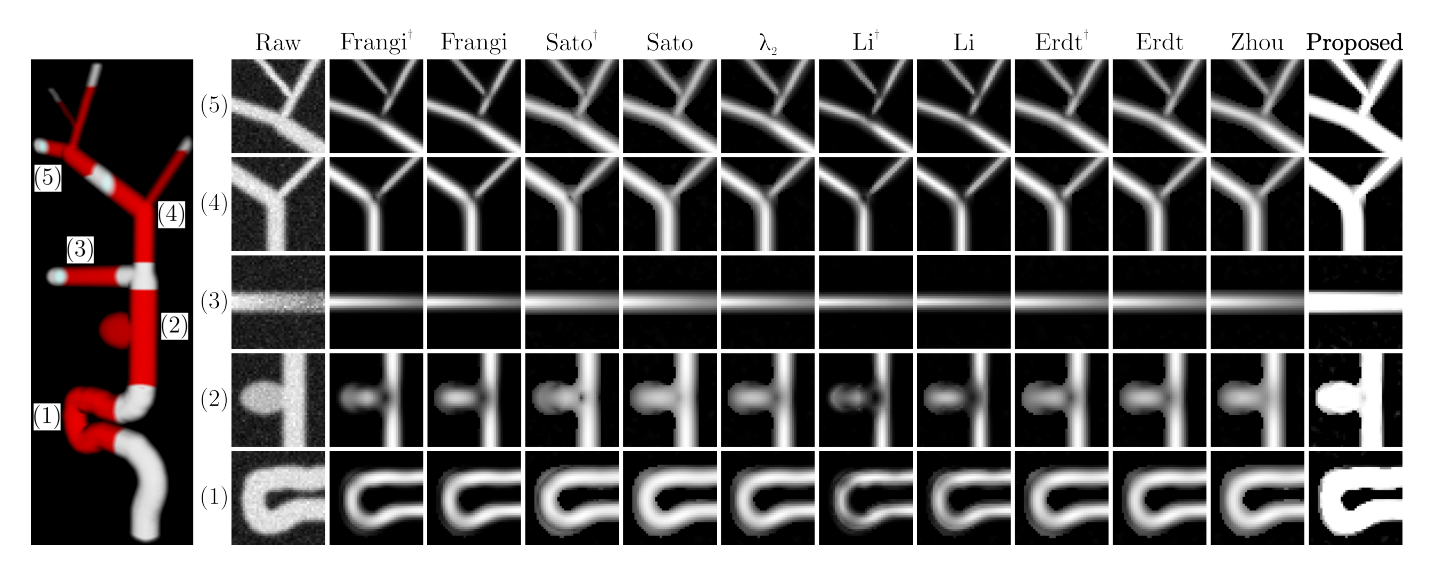


Fig. 1. Volume rendering of a synthetic vasculature with five typical structures and appearances: (1) bent (curved) vessel, (2) aneurysm, (3) vessel with varying contrast, (4) bifurcation and (5) vessels of various diameters. Image patches in rows 1–5 correspond to medial cross-sections of synthetic vasculature either of raw intensity or enhanced with multiscale filter based on a novel and several established enhancement functions. Responses of original Frangi's, Sato's, Li's and Erdt's functions, which suppress rounded structures, are marked with †. All responses were computed across the same range of scales.

methods which are based on gradient vector flow [20] or oriented flux [21]. Due to high resistance to image noise, matched filters [22], [23] are widely used on 2D images as an alternative to the Hessian based filters. However, matched filters require a high number of orientation kernels, which makes them less suitable for use on 3D images.

Structural image filters based on Hessian analysis seem to be the most popular. Their recent applications include segmentation of liver vessels in abdominal CTA [24] and lung vessels in thoracic CT [25]; extraction of coronary vasculature from cryomicrotome images [26]; extraction of vessel centerlines from CTA and contrast enhanced X-ray for 2D/3D coronary artery registration [27]; detection of mesenteric vasculature in CTA for small bowel segmentation [28]; detection and quantification of coronary artery stenoses in CTA [6]; and computer-aided detection of cerebral aneurysms in 3D rotational angiography, CTA and MRA [7].

In Hessian based filtering a certain enhancement function is maximized across a Gaussian scale space of the angiographic image. The enhancement function most frequently applied is Frangi's [13]. Different, but less applied functions are Sato's [14], Li's [15], Erdt's [16] and Zhou's [17]. Most of these functions were devised for the enhancement of 3D images, while Frangi's and Zhou's can also be used for the enhancement of 2D images. An ideal enhancement function should exhibit a high and uniform response to i) variable vascular morphology, e.g. straight and bending vessels, vessels of different dimensions and cross-sections (circular-elliptical), and bifurcations or crossings, ii) pathology (e.g. blob-like aneurysms), iii) blood flow/contrast agent induced intensity non-uniformities within and across vessels, iv) blurring of the vessel boundary and v) image noise. Unfortunately, the established enhancement functions are far from ideal (Fig. 1), which may compromise subsequent analysis of the enhanced

Based on our previous work [29], we advance the multi-

scale Hessian filtering by a novel enhancement function, which overcomes the deficiencies of the established functions and has properties close to an ideal enhancement function. Compared to [29], more detailed descriptions of the novel 3D enhancement function and its extension to 2D are presented. Furthermore, several established enhancement functions are thoroughly reviewed and their performances evaluated on several clinical 3D and 2D angiographic modalities to demonstrate the benefits of the novel function for the enhancement of vascular structures.

Quantitative evaluation was performed on three clinical image datasets where the first consisted of 3D thoracic CT images of lung vasculature, the second of 3D-DSAs of cerebral vasculature and the third of high resolution 2D color images of fundus. The results on all three datasets showed that, compared to the established functions, the proposed 3D and 2D enhancement functions have a higher and more uniform response for variable vascular morphology, vascular pathology like aneurysm, and intensity non-uniformities within and across vessels. The same conclusions were made based on visual assessment of enhanced cerebral 3D time-of-flight (TOF)-MRA, a 3D-DSA image of cerebral aneurysm and contrast enhanced 2D X-ray of the cerebral vasculature.

The paper is organized as follows: Section II reviews the Hessian-based multiscale filters and established enhancement functions and their drawbacks, while Section III introduces a novel enhancement function. Clinical image datasets of lung, cerebral and fundus vascular structures, and the experiments and results of the evaluation of enhancement filters are described in Section IV. Discussion and conclusion are given in Section V.

II. BACKGROUND

Enhancement filters based on the analysis of eigenvalues of the Hessian matrix applied on a D-dimensional image are functions $\mathcal{V}: \mathbb{R}^D \to \mathbb{R}$, which selectively amplify a specific

local intensity profile or structure in an image. A class of enhancement filters [13]–[17] distinguish between different local structures by analyzing the second order intensity derivatives or Hessian at each point in the image. To enhance the local structures of various sizes, the analysis is typically performed on a Gaussian scale space of the image.

Let $I(\mathbf{x})$ denote the intensity of a D-dimensional image at coordinate $\mathbf{x} = [x_1, \dots, x_D]^T$. The Hessian of $I(\mathbf{x})$ at \mathbf{x} and scale s is then represented by a $D \times D$ matrix:

$$H_{ij}(\mathbf{x}, s) = s^2 I(\mathbf{x}) * \frac{\partial^2}{\partial x_i \partial x_j} G(\mathbf{x}, s) \text{ for } i, j = 1, ..., D, (1)$$

where $G(\mathbf{x}, s) = (2\pi s^2)^{-D/2} \exp(-\mathbf{x}^T \mathbf{x}/2s^2)$ is a *D*-variate Gaussian and * denotes convolution.

Selective enhancement of local image structures that is independent of orientation and based on shape and foreground versus background brightness of the structures can be performed by analyzing the signs and magnitudes of Hessian eigenvalues. For each \mathbf{x} , the eigenvalues are obtained through eigenvalue decomposition eig $\mathcal{H}(\mathbf{x},s) \to \lambda_i, i=1,\ldots,D$, which can be computed fast for 2×2 or 3×3 Hessian matrices in either 2D or 3D images, respectively, with the analytical method proposed by Kopp [30].

Ideally, the Hessian-based enhancement is a response of an indicator function $\mathbf{1}_{ER}: \big[\operatorname{eig}\mathcal{H}(\mathbf{x},s)\big] \to \{0,1\}$ of a certain set of eigenvalue relations ER. For example, elongated tubelike structures such as vessels in 3D images (D=3) can be enhanced by functions indicating: $\lambda_2 \approx \lambda_3 \wedge |\lambda_{2,3}| \gg |\lambda_1|$, where the eigenvalues λ_i of $\mathcal{H}(\mathbf{x},s)$ are sorted according to their magnitudes: $|\lambda_i| \leq |\lambda_{i+1}|; i=1,\ldots,D-1$. The positive (negative) signs of λ_2 and λ_3 indicate a dark (bright) structure on a bright (dark) background. In 2D images (D=2), elongated structures are indicated by: $|\lambda_2| \gg |\lambda_1|$, whereas the sign of λ_2 indicates a bright (dark) structure on dark (bright) background. For differently shaped structures the eigenvalue relations can be obtained in a similar manner.

To cope with variations of shape and intensity of the targeted structures, image noise, etc. the indicator functions $\mathbf{1}_{ER}$ are approximated by smooth enhancement functions \mathcal{V} : $\left[\operatorname{eig}\mathcal{H}(\mathbf{x},s)\right] \to \mathbb{R}_0^+$, which have a non-negative response. A multiscale filter response $\mathcal{F}(\mathbf{x})$ is then obtained by maximizing a given enhancement function \mathcal{V} , at each point \mathbf{x} , over a range of scales s as:

$$\mathcal{F}(\mathbf{x}) = \sup \Big\{ \mathcal{V} \big[\operatorname{eig} \mathcal{H}(\mathbf{x}, s) \big] : s_{\min} \le s \le s_{\max} \Big\}.$$
 (2)

The values of s_{\min} and s_{\max} are selected according to the respective minimal and maximal expected size of the structures of interest.

A. Enhancement of Vascular Structures

The vasculature mainly consist of straight vessels and rounded structures like bending vessels, bifurcations and vascular pathologies such as aneurysms.

To simultaneously enhance both elongated and rounded structures in 3D the function V should indicate the following Hessian eigenvalue relations:

$$\mathbf{1}_{ER}: \lambda_2 \approx \lambda_3 \wedge |\lambda_{2,3}| \gg |\lambda_1|. \tag{3}$$

In 2D, the indicator function is defined as $|\lambda_2| \gg |\lambda_1|$.

As vessel enhancement functions \mathcal{V} were primarily devised to enhance elongated structures, they contain a component that is aimed to suppress rounded structures. However, because not all vascular structures are elongated, this is a serious drawback, which is discussed in more detail in the next subsection. Here we review several enhancement functions and modify certain original expressions by removing suppression of rounded structures. In this way, all the presented expressions account for the indicator function in (3). As most established functions were designed to enhance 3D images, we developed the corresponding expressions for enhancing 2D images by substituting $\lambda_3 = \lambda_2$ in the 3D enhancement functions and then simplifying the expressions. The underlying assumption made when deriving the 2D equivalents of the 3D enhancement function is that vessels (and other vascular structures) have a circular cross-section in 3D, a situation in which the eigenvalues λ_3 and λ_2 are equal.

Based on the relative brightness of the vascular structures compared to the background, the enhancement functions $\mathcal V$ yield a non-zero response only when a specific relation between the eigenvalues λ_i is satisfied. For bright vascular structures on a dark background ($\lambda_i < 0, \forall i$), $\mathcal V$ has a nonnegative response when $\lambda_3 \leq \lambda_2 < 0$ for D=3 and $\lambda_2 < 0$ for D=2, or zero otherwise. Conversely, for vascular structures darker than background ($\lambda_i > 0, \forall i$), the enhancement functions $\mathcal V$ yield a non-negative response when $\lambda_3 \geq \lambda_2 > 0$ for D=3 and $\lambda_2 > 0$ for D=2. If not noted otherwise, the same enhancement function $\mathcal V$ can be used irrespective of the relative brightness of the structures of interest, however, the correct assumption for the relation between eigenvalues λ_i needs to be considered.

The most widely used function is Frangi's [13], in which the factor $\exp\left(-\frac{\mathcal{R}_{\mathcal{B}}^2}{2\beta^2}\right)$, with $\mathcal{R}_{\mathcal{B}}=|\lambda_1|/\sqrt{\lambda_2\lambda_3}$ and $\beta=\mathrm{const}$, suppresses rounded structures. By removing this factor, we obtain the following function:

$$V_{\rm F} = \left(1 - \exp\left(-\frac{\mathcal{R}_{\rm A}^2}{2\alpha^2}\right)\right) \left(1 - \exp\left(-\frac{\mathcal{S}_3^2}{2\kappa^2}\right)\right), \quad (4)$$

where $S_3 = \sqrt{\lambda_1^2 + \lambda_2^2 + \lambda_3^2}$ is the 2nd order measure of image structureness, which is defined as $S_D = \sqrt{\sum_{i \leq D} \lambda_i^2}$, where D denotes dimension, and $\mathcal{R}_A = \lambda_2/\lambda_3$ distinguishes between tubular and planar structures. Parameters α and κ control the sensitivity of measures \mathcal{R}_A and \mathcal{S} , respectively. In 2D, the corresponding modified Frangi's enhancement function consists only of the second factor of (4), i.e. $\mathcal{V}_F = 1 - \exp\left(-\mathcal{S}^2/2\kappa^2\right)$, where $S_2 = \sqrt{\lambda_1^2 + \lambda_2^2}$.

The original Sato's enhancement function [14] contains the factor $(1 + \frac{\lambda_1}{|\lambda_2|})^{\delta}$, $\delta \ge 0$ to suppress rounded structures. By removing this factor we get:

$$V_{\rm S} = |\lambda_3| \left(\frac{\lambda_2}{\lambda_3}\right)^{\gamma} \,. \tag{5}$$

The parameter γ controls the sensitivity to elongated structures and is typically set to 0.5 or 1, which simplifies the expression (5) to $\sqrt{\lambda_3\lambda_2}$ or $|\lambda_2|$, respectively. We will refer to the former

as Sato's enhancement function and to the latter as $|\lambda_2|$. In 2D, Sato's function reduces to $|\lambda_2|$.

The enhancement function proposed by Li *et al.* [15] contains an additive term $-|\lambda_2| \times (\lambda_1/\lambda_3)$ for suppression of rounded structures, which when removed yields:

$$\mathcal{V}_{L} = |\lambda_{2}| \times \frac{\lambda_{2}}{\lambda_{3}}.$$
 (6)

The first factor represents the magnitude and the second the likelihood of an elongated and rounded structure, since $\lambda_2/\lambda_3 \rightarrow 0$ in case of plane-like or no structure. In 2D, similarly as Sato's, Li's function reduces to $|\lambda_2|$.

Erdt's enhancement function [16] suppresses rounded structures by an additive term $+\frac{2}{3}K\lambda_1$, which when removed yields:

$$\mathcal{V}_{\rm E} = K \left| -\lambda_2 - \lambda_3 \right| \,, \tag{7}$$

where $K=1-|\lambda_2-\lambda_3|/|\lambda_2+\lambda_3|$ is a cross-sectional isotropy factor that approaches zero for plane-like structures $(|\lambda_3|\gg |\lambda_{1,2}|)$ or one otherwise. In 2D, similarly as Sato's and Li's, Erdt's function reduces to $|\lambda_2|$.

To enhance both rounded and elongated structures, Zhou *et al.* [17] proposed the following function:

$$V_{\rm Z} = \frac{|\lambda_2 + \lambda_3|}{2} \times \exp\left(-\left|\frac{|\lambda_3|}{S_3} - c\right|\right),$$
 (8)

where parameter c is between $\frac{1}{\sqrt{3}}$ and $\frac{1}{\sqrt{2}}$ and \mathcal{S} is the structureness measure as in (4). The equivalent function in 2D is $\mathcal{V}_{\rm Z} = |\lambda_2| \times \exp\left(-||\lambda_2|/\mathcal{S}_2 - c|\right)$ with c between $\frac{1}{\sqrt{2}}$ and 1.

B. Deficiencies of Enhancement Functions

Fig. 1 shows a 3D rendering of synthetic vasculature with five typical structures and appearances: (1) a bent (curved) vessel, (2) an aneurysm, (3) a vessel with varying contrast, (4) a bifurcation and (5) vessels of various diameters. Image patches in rows 1-5 correspond to medial cross-sections of synthetic vasculature either of the raw intensity or enhanced with multiscale filter based on six established and a novel enhancement function. To demonstrate the impact of suppression of rounded structures by original Frangi's, Sato's, Li's and Erdt's enhancement functions their responses marked with † are also shown. It is evident that the suppression of rounded structures results in a rather poor response within the aneurysm and at vessel bends and bifurcations. Despite the removal of rounded-structure suppression component the responses obtained by (4–7), and Zhou's function (8) still demonstrate several deficiencies: i) a varying and eroded response at bents (row 1), ii) a poor response at the aneurysm, especially at the neck (row 2), iii) response affected by non-uniform intensities (row 3), iv) a poor response at the bifurcations (rows 4 and 5), and v) sensitivity to vessel size (row 5).

One of the main reasons for the observed deficiencies is that the established enhancement functions are proportional to the magnitude or squared magnitude of λ_2 or λ_3 , or both. By using $e^x \approx 1 + x$ to approximate the second factor in (4) we get:

$$\left(1 - \exp\left(-\frac{S^2}{2\kappa^2}\right)\right) \approx \frac{1}{2\kappa^2} \left(\lambda_1^2 + \lambda_2^2 + \lambda_3^2\right), \quad (9)$$

This shows that Frangi's function (4) is also proportional to the squared magnitude of λ_2 and λ_3 . The main reason for designing enhancement functions proportional to the magnitude of eigenvalues was to suppress noise in image regions with low and uniform intensities, where all the eigenvalues have low and similar magnitudes.

Responses of enhancement functions that are directly proportional to λ_2 or λ_3 magnitudes have three important drawbacks. First, for an ideal elongated or rounded structure of uniform intensity, the response of λ_2 or λ_3 is not uniform within the structure (see λ_2 in Fig. 1). The response peaks at the center of the structure and then progressively decreases towards the periphery. Second, as varying image intensities result in varying λ_2 and λ_3 magnitudes the functions' responses are non-uniform. Third, the filter response depends on the structure size because the enhancement is not uniform across scales.

Another drawback is that the current indicator function (3) leads to suppression of structures with non-circular cross-sections (e.g. elliptic), because the ratio λ_2/λ_3 corresponds to the ratio of minor and major semi axes of a structure's cross-section. This ratio will be one for circular and less than one for elliptic cross-sections.

III. NOVEL ENHANCEMENT FUNCTION

We hypothesize that an enhancement function: i) in the form of a ratio of eigenvalues, ii) robust to low-magnitudes of eigenvalues, and iii) accounting for structures with elliptic cross-sections will yield a more uniform response across different vascular structures than the existing functions. In the following we introduce such an enhancement function for 3D and 2D vascular images.

A. Enhancement in 3D

Enhancement of vascular structures is dependent on their relative brightness compared to the surrounding background. A general enhancement function can be developed by redefining the Hessian eigenvalues with respect to the brightness of the structures of interest (dark or bright compared to the background). Each eigenvalue λ_i ; i = 1, 2, 3 is redefined as:

$$\lambda_i := \begin{cases} -\lambda_i & \text{bright structures on dark background}, \\ \lambda_i & \text{dark structures on bright background}. \end{cases}$$
 (10)

Peeters et al. [31] reviewed several measures of structural isotropy and anisotropy of diffusion tensors, some of which can also be applied to Hessian matrices. A measure based on the ratio of eigenvalues, that is otherwise used for the detection of nearly spherical diffusion tensors [32], is volume ratio:

$$VR = |\lambda_1 \lambda_2 \lambda_3| \left[\frac{3}{|\lambda_1| + |\lambda_2| + |\lambda_3|} \right]^3, \tag{11}$$

which was modified from the original version by adding absolute values to account for differently signed eigenvalues. The response of such VR is between 0 and 1.

We start building our enhancement function on (11). To indicate elongated structures, for which $|\lambda_1| \ll |\lambda_2|$, the VR

is modified by substituting $\lambda_1 \to (\lambda_2 - \lambda_1)$, which results in a function that enhances elongated structures like vessels:

$$\mathcal{V} = |(\lambda_2 - \lambda_1) \lambda_2 \lambda_3| \left[\frac{3}{|2\lambda_2 - \lambda_1| + |\lambda_3|} \right]^3. \tag{12}$$

This function would suppress rounded structures, because their characteristic eigenvalue relation is $\lambda_1 \approx \lambda_2 \approx \lambda_3$ and the multiplicative factor $(\lambda_2 - \lambda_1)$ in (12) would be zero or close to zero for rounded structures. Since vascular structures may be elongated or rounded, an enhancement function is required that would enhance both. Such a function is obtained by eliminating λ_1 from the multiplicative factor in (12) and, to ensure normalized function response, from the denominator in the last factor. Furthermore, the resulting function depends only on λ_2 and λ_3 , which is consistent with the indicator function (3) for vascular structures.

The response of such an enhancement function, however, is ill-defined at low magnitudes of λ_2 and λ_3 and thus too susceptible to noise in image regions of uniform intensity. To ensure robustness of the enhancement function to low-magnitudes of λ_2 and λ_3 , we propose to regularize the value of λ_3 at each scale s as:

$$\lambda_{\rho}(s) = \begin{cases} \lambda_{3} & \text{if } \lambda_{3} > \tau \max_{\mathbf{x}} \lambda_{3}(\mathbf{x}, s), \\ \tau \max_{\mathbf{x}} \lambda_{3}(\mathbf{x}, s) & \text{if } 0 < \lambda_{3} \leq \tau \max_{\mathbf{x}} \lambda_{3}(\mathbf{x}, s), \\ 0 & \text{otherwise}, \end{cases}$$

where τ is a cutoff threshold between zero and one. To normalize the response of proposed enhancement function across the scales, λ_{ρ} is computed for each scale s separately. For structures of very low contrast, which otherwise have low magnitude of λ_2 and λ_3 , choosing a high value of τ results in a high difference between the magnitudes of λ_2 and λ_{ρ} and thus supresses the response.

With the above eigenvalue regularization, the enhancement function can be written independently of the relative brightness of the structures of interest as:

$$\mathcal{V} = \lambda_2^2 \,\lambda_\rho \, \left[\frac{3}{2\lambda_2 + \lambda_\rho} \right]^3, \tag{14}$$

which is valid only when the condition $\lambda_2 > 0 \land \lambda_\rho > 0$ can be satisfied. In the opposite case the response is set to $\mathcal{V} = 0$.

To enhance vascular structures with elliptic cross-sections the function in (14) should, instead of $\lambda_2 \approx \lambda_\rho$, indicate the relation $\lambda_2 \leq \lambda_\rho$. By indicating the eigenvalue relation $\lambda_2 \geq \lambda_\rho/2$ we account for structures with elliptic cross-sections with ratio of λ_2/λ_ρ from 0.5 to 1. This can be achieved by substituting $\lambda_\rho \to (\lambda_\rho - \lambda_2)$ in (14) and fixing the response to 1 for $\lambda_2 \geq \lambda_\rho/2 > 0$. Finally, the proposed enhancement function is computed as:

$$\mathcal{V}_{P} = \begin{cases}
0 & \text{if } \lambda_{2} \leq 0 \lor \lambda_{\rho} \leq 0, \\
1 & \text{if } \lambda_{2} \geq \lambda_{\rho}/2 > 0, \\
\lambda_{2}^{2} \left(\lambda_{\rho} - \lambda_{2}\right) \left[\frac{3}{\lambda_{2} + \lambda_{\rho}}\right]^{3} & \text{otherwise},
\end{cases} (15)$$

where λ_{ρ} is computed by (13). The proposed enhancement function \mathcal{V}_{P} can be computed for both bright structures on dark background and dark structures on white background if

the eigenvalues are redefined by (10). The multiscale filter response (2) based on this enhancement function is between 0 and 1 and is, ideally, 0 for non-vascular and 1 for vascular structures.

As hypothesized, the proposed enhancement function yields the highest and most uniform response on typical vascular structures that are synthesized in Fig. 1.

B. Enhancement in 2D

The proposed function \mathcal{V}_P in (15) can also be adopted to 2D images (D=2). Besides the two computed eigenvalues λ_1 and λ_2 ($|\lambda_2| \geq |\lambda_1|$), which need to be redefined according to (10), we introduce an auxiliary λ_3 , which is set to λ_2 . This definition of λ_3 on the 2D images implies the assumption that in 3D the vessels and other vascular structures have a circular cross-section. Using $\lambda_3 = \lambda_2$ in (13) yields a regularized eigenvalue λ_ρ , which is employed in (15) together with λ_2 to compute the response of the proposed enhancement function \mathcal{V}_P on a 2D image.

IV. EXPERIMENTS AND RESULTS

The enhancement of vascular structures by the multiscale filter (2) based on several established and the proposed enhancement functions was quantitatively and qualitatively evaluated on clinical images of lung, cerebral and fundus vasculatures. The functions were applied to enhance normal vascular structures such as small- and large-diameter vessels and bifurcations, as well as vascular pathologies like aneurysms. The clinical image datasets and experiments are described in the following subsections.

A. Thoracic CT Images

A database of 20 thoracic computed tomography (CT) images with binary lung masks was obtained from the VES-SEL12 grand challenge [25], which is a public platform for evaluating the performance of methods for segmentation of vascular structures of the lungs in thoracic CT images. The CTs were acquired on a variety of clinical scanners and with different protocols. Approximately half of the CTs were acquired with contrast agent injected into the blood flow. Besides, about half of the CT images contained abnormalities such as emphysema, nodules or pulmonary embolisms. The size of CT images was $512 \times 512 \times 355-543$ and most were isotropic with up to a 1 mm spacing between axial slices.

For evaluating a segmentation of vascular structures, the CT images contained landmarks manually annotated by expert radiologists. The 20 CT images contained 7352 landmarks, of which 2238 and 5114 were annotated on vascular and non-vascular structures, respectively. The landmarks were not disseminated with the CT images, thus the obtained segmentations had to be submitted through the grand challenge website for evaluation. The segmentation of vascular structures can be either binary or probabilistic (i.e. voxel-wise likelihood).

Based on annotated landmarks the performance of a vessel segmentation is evaluated on each CT image by computing

¹VESSEL12 website: http://vessel12.grand-challenge.org/

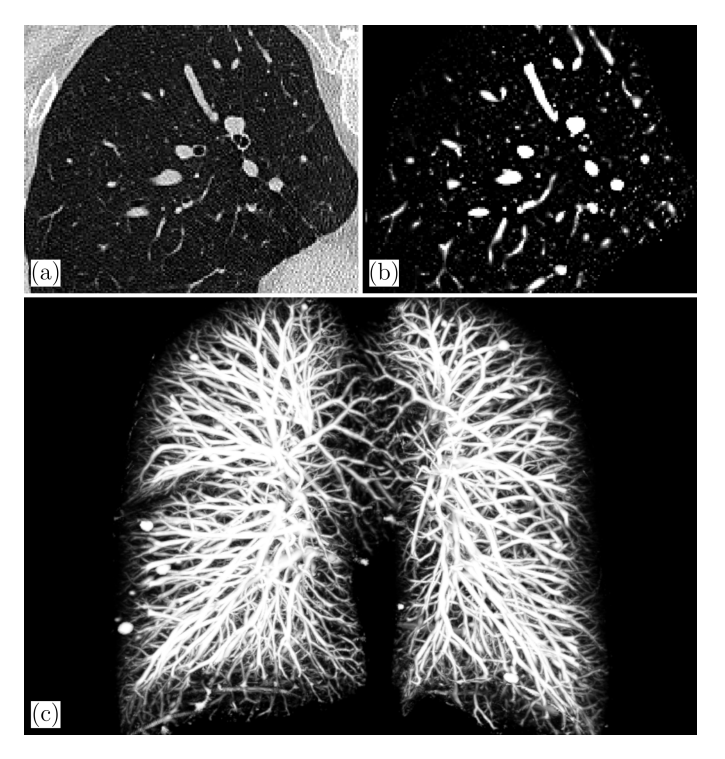


Fig. 2. Enhancement of the lung region in a thoracic CT from the VESSEL12 image database [25]: (a) axial slice of a CT image and (b) response of the proposed filter. The enhanced lung vasculature (c) visualized in 3D by maximum intensity projection. (see video 1 in Supplemental material)

area under the receiver operating characteristic (ROC) curve (AUC) [33], sensitivity (SE) and specificity (SP). For a probabilistic segmentation, the SE and SP are reported at an optimal threshold, which is determined by a point on the ROC curve closest to the optimal classifier (i.e. upper left corner of ROC graph). The range of metrics AUC, SE and SP is between 0 and 1, where values closer to 1 indicate a better segmentation. Methods are ranked according to overall highest AUC.

The response of the proposed filter for $\tau=1$ was computed within the lung mask provided with the database and simply scaled to $[0,\,255]$ to obtain a probabilistic segmentation, which was submitted for evaluation. The response was computed over scales between $s_{\rm min}=0.9$ and $s_{\rm max}=3$ mm with step size of 0.7 mm, which were chosen similar to the scales used in Hessian-based enhancement filters previously evaluated in the VESSEL12 challenge [25].

Evaluation results for the top six teams according to the AUC ranking [25] are shown in Table I. The team that ranked first based their method on learning stacked multiscale features, which were used to train the L2-regularized logistic regression classifier for vessel extraction [34]. The remaining five teams employed the multiscale Hessian-based filter (2). The filter in combination with the proposed enhancement function ($\tau=1$) achieved a tied AUC of 0.984 with the segmentations submitted by teams LKEBChina and FME_LungVessels. Team LKEBChina modified a vessel medialness function [12] into a vessel enhancement function, while the other teams used the Frangi's vesselness function [13] extended with region growing based on fuzzy connectivity (FME LungVessels) or variational region growing (CREALUNG), or used optimiza-

TABLE I
THE TOP SIX SEGMENTATIONS REPORTED ON VESSEL12
CHALLENGE [25] WEBSITE[†]. RANKING IS BASED ON THE AUC.

Rank	Team Name	AUC	SE	SP
1	UofA_vision	0.986	0.949	0.941
2	LIT (Proposed, $\tau = 1$)	0.984	0.962	0.961
2	LKEBChina	0.984	0.953	0.956
2	FME_LungVessels	0.984	0.954	0.937
5	Bahcesehir University	0.980	0.954	0.947
6	CREALUNG	0.972	0.953	0.935

[†] Last accessed on: December 31, 2015

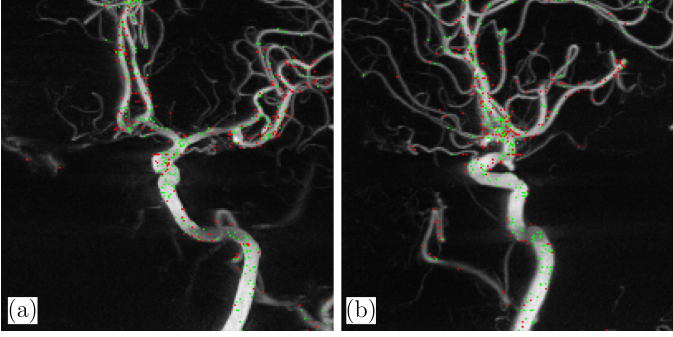


Fig. 3. (a) Lateral and (b) anterior-posterior maximum intensity projection of a 3D-DSA with landmark positions annotated as vascular (*green points*) or non-vascular (*red points*). (see video 2 in Supplemental material)

tion of the scale range based on training datasets (Bahcesehir University). The mentioned extensions, which were applied to the enhanced images, aimed to increase the otherwise low SP of segmentations obtained by enhancement filters. Nevertheless, the segmentations based simply on responses obtained with the proposed enhancement function resulted in highest overall SE and SP, even in comparison to the best method according to AUC.

Fig. 2 shows a slice of a CT image from the VESSEL12 database and the multiscale response of proposed enhancement function. The response has similar intensity on large and small vessels and is uniform within the vessels, which can be exploited for visualization of the whole lung vasculature by fast 3D volume rendering (Fig. 2c). Such a visualization facilitates navigation through the vasculature and identification of possible vascular pathologies [11].

B. Cerebral 3D-DSA Images

Twenty patients undergoing endovascular treatment of cerebral aneurysms were imaged by the Siemens Axiom Artis dBA angiography system. For each patient, a 3D-DSA of size $512 \times 512 \times 391$ voxels and 0.46 mm isotropic spacing was acquired. In each 3D-DSA a volume of interest (VOI) of size $200 \times 200 \times 200$ voxels was manually selected such that it contained the cerebral vasculature.

Evaluation of the multiscale filter (2) with seven enhancement functions: the proposed (15), Frangi's (4), Sato's (5), λ_2 , Li's (6), Erdt's (7) and Zhou's (8) was based on annotated landmarks, similarly as in the VESSEL12 challenge. For each

TABLE II
MEAN VALUES OF EVALUATION METRICS FOR THE ENHANCEMENT RESPONSES COMPUTED OVER 20 CEREBRAL 3D-DSA IMAGES.

Filter	AUC	SE	SP	MedNR
Frangi [†]	0.944	0.875	0.904	0.34
Frangi	0.934	0.871	0.890	0.37
Sato [†]	0.941	0.884	0.870	0.24
Sato	0.941	0.890	0.863	0.25
Li [†]	0.910	0.832	0.845	0.12
Li	0.906	0.817	0.865	0.14
Erdt [†]	0.931	0.864	0.880	0.20
Erdt	0.940	0.886	0.890	0.20
λ_2	0.940	0.886	0.890	0.20
Zhou	0.934	0.895	0.855	0.24
Proposed ($\tau = 0.5$)	0.953	0.895	0.909	0.96
Proposed $(\tau = 1)$	0.954	0.896	0.909	0.55

[†] Original functions, which suppress rounded structures.

3D-DSA image an expert radiologist placed and annotated 250 landmarks on vascular and 250 in the vicinity of vascular structures like bifurcations, aneurysms, highly bent vessels, etc., and in between neighboring vessels, where the responses of enhancement functions were expected to differ most. Fig. 3 shows a set of landmarks superimposed onto a maximum intensity projection (MIP) of a 3D-DSA.

Evaluation of the obtained filter responses was based on metrics AUC, SE and SP, computed in the same way as for the responses on thoracic CT images. To measure the uniformity of the responses on vascular structures, we introduced a fourth metric, computed as the median of normalized responses (MedNR) across the landmark positions on vascular structures. The range of metric MedNR is between 0 and 1, where the values closer to 1 indicate a more uniform filter response on vascular structures.

The proposed function was tested by varying τ from 0 to 1. Parameters κ and α of Frangi's (4) and c of Zhou's (8) were tuned so as to maximize the mean value of evaluation metrics computed over all 20 3D-DSAs. The obtained optimal values were $\kappa = 0.05 \cdot \max_{\mathbf{x}} I(\mathbf{x}), \ \alpha = 0.5$ and c = 0.7. For each of the tested functions, the multiscale filter response (2) was computed over scales from $s_{\min} = 0.5$ to $s_{\max} = 2.5$ mm with a step of 0.5 mm. The obtained responses were scaled between 0 and 1 to obtain a probabilistic segmentation.

Table II reports the mean AUC, SE, SP, and MedNR values obtained across 20 cerebral 3D-DSA images for the multiscale filter responses based on the proposed ($\tau = \{0.5, 1\}$) and six other enhancement functions. Moreover, for Frangi's, Sato's, Li's, and Erdt's modified filters we report also the metrics for their original variants (†), which suppress rounded structures. While there was only a small difference in AUC, SE, and SP metrics between the original and modified versions of the four filters, the original filters had lower MedNR values. This indicates a lower response uniformity across the vascular structures, mainly because in the original functions the response is suppressed at bifurcations and aneurysms. The proposed function achieved the highest AUC, SE, and

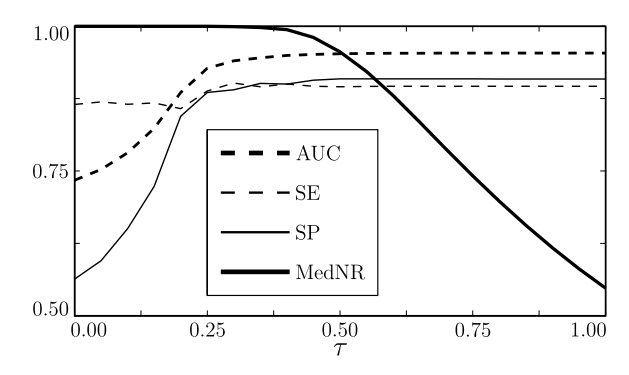


Fig. 4. Mean values of AUC, SE, SP and MedNR metrics, computed for the responses of multiscale filter with the proposed enhancement function, over 20 cerebral 3D-DSA images shown with respect to parameter τ (13).

SP (best segmentation performance) and the highest MedNR (most uniform response on vascular structures). In general, lowering τ of the proposed function from 1 to 0.5 only slighly decreased the means of AUC and SE, SP did not change, while the mean of MedNR increased substantially.

For the multiscale filter based on the proposed enhancement function, Fig. 4 shows the influence of regularization parameter τ varied from 0 to 1 on the mean of AUC, SE, SP, and MedNR, computed across 20 cerebral 3D-DSA images. When τ is 0, the magnitude of λ_3 is not regularized through (13) and the response of (15) is very sensitive to image noise. This causes a higher number of false positive responses, which effectively lower both SP and AUC. At the same time, the response is nearly uniform on vascular structures as even the structures with very low contrast are enhanced, thus, the MedNR is close to 1. For $\tau < 0.4$ the MedNR is flat at 1 and then progressively decreases when τ increases beyond 0.4. Increasing τ up to 0.25 notably increases the AUC and SP, and slightly the SE, which then all flatten out when $\tau > 0.4$. Because the values of AUC, SE, and SP are flat beyond $\tau > 0.4$, we recommend that τ is set somewhere in range from 0.5 to 1. One should set τ to 1 for the purpose of segmentation (highest AUC, SE and SP) and to 0.5 to maximize response uniformity on vascular structures, which can be exploited for fast 3D volume rendering (Fig. 2c).

Fig. 5 shows the MIP of a cerebral 3D-DSA and corresponding MIPs of multiscale filter responses for the seven tested enhancement functions. The response of proposed function is high and highly uniform across all vascular structures, as indicated by high mean MedNR in Table II, thus the MIP for the proposed function appears brighter as compared to MIPs obtained with other enhancement functions. Within aneurysms shown in Fig. 5, MIP based on the proposed function had highly uniform intensity throughout the area of the two aneurysm, while the MIPs of other functions had highest intensity in the aneurysm's center and lower towards its boundary.

C. High-Resolution 2D Fundus Images

The 2D multiscale enhancement filters were evaluated on the publicly available High-Resolution Fundus (HRF) image

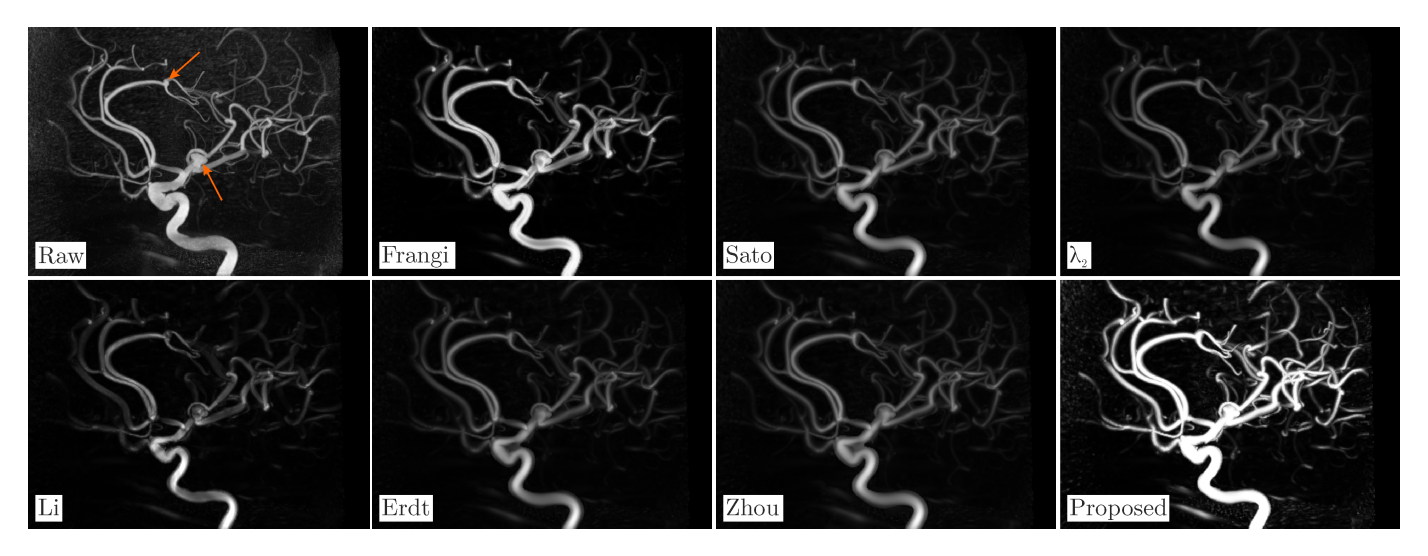


Fig. 5. Maximum intensity projections of a raw 3D-DSA and multiscale filter responses of several established and proposed enhancement functions. Arrows in the Raw image point to two aneurysms.

TABLE III

MEAN VALUES OF EVALUATION METRICS FOR THE 2D ENHANCEMENT
FILTERS AND A SEGMENTATION METHOD BASED ON MATCHED
ENHANCEMENT FILTER [28] OVER 45 HRF COLOR IMAGES, WHERE SE
AND SP REPRESENT THE POINT IN ROC CURVE WITH THE HIGHEST ACC.

Method	AUC	ACC	SE	SP	MedNR
Frangi	0.941	0.949	0.608	0.982	0.50
λ_2	0.942	0.950	0.617	0.982	0.19
Zhou	0.943	0.951	0.622	0.983	0.19
Proposed $(\tau = 0.5)$	0.943	0.954	0.651	0.983	0.97
Proposed $(\tau = 1)$	0.944	0.954	0.646	0.983	0.62
Odstrcilik [23]	0.968	0.949	0.774	0.967	_

database² [23], which consists of three datasets, one of healthy subjects, one of patients with diabetic retinopathy and one of patients with glaucoma. Altogether, the three datasets contain 45 color HRF images, each of size 3504×2336 . All 45 images were used for evaluating the 2D enhancement filters.

Enhancement of vascular structures was performed on the green channel intensity of each of the 45 HRF images. Four enhancement functions were tested: the proposed, Frangi's, λ_2 and Zhou's. Note that the expressions for Sato's (5), Li's (6) and Erdt's (7) enhancement functions in 3D all reduce to λ_2 in 2D. The proposed enhancement function was tested by varying τ from 0 to 1. Parameters κ and α of Frangi's (4) and c of Zhou's (8) function were tuned so as to maximize the mean value of evaluation metrics computed over all 45 HRF images. The obtained optimal values were $\kappa=0.05\cdot\max_{\mathbf{x}}I(\mathbf{x}),$ $\alpha=0.5$ and c=1. For each tested enhancement function, the multiscale filter response (2) was computed over scales from $s_{\min}=4$ to $s_{\max}=15$ pixels with step 0.5.

The responses of enhancement filters on HRF images were evaluated based on reference manual segmentations of vascular structures provided by the authors of the HRF

TABLE IV

MEAN VALUES OF EVALUATION METRICS FOR THE 2D ENHANCEMENT FILTERS OVER 45 HRF COLOR IMAGES, WHERE SE AND SP REPRESENT THE POINT CLOSEST TO THE IDEAL POINT IN ROC CURVE.

Method	AUC	SE	SP	MedNR
Frangi	0.941	0.896	0.898	0.50
λ_2	0.942	0.897	0.900	0.19
Zhou	0.943	0.896	0.902	0.19
Proposed $(\tau = 0.5)$	0.943	0.895	0.906	0.98
$\textbf{Proposed} (\tau=1)$	0.944	0.895	0.906	0.65

image database [23]. As in their comparative study [23], we computed AUC, SE and SP for each response. Besides, MedNR was computed on pixels belonging to the reference segmentation. For a 2D probabilistic segmentation, the values of SE and SP are reported for a threshold obtained at the highest segmentation accuracy (ACC).

The mean of AUC, ACC, SE, SP and MedNR computed for multiscale filter responses across 45 2D HRF images are summarized in Table III. In the table, we also report the best segmentation result on 45 HRF images reported in a previous study [23], wherein a matched enhancement filter that employed oriented vessel patches and morphologic post-processing achieved the highest AUC of 0.968.

Reporting the values of SE and SP obtained at the threshold with the highest ACC is a standard procedure in the community of fundus segmentation methods [23], however, it produces unbalanced results where a higher SP is favored because vessels cover a considerably lower amount of the image compared to the background. Consequently, additional results are displayed in Table IV, where SE and SP are computed as the point on the ROC curve closest to the ideal point (SE=1, SP=0), which produces a more balance evaluation, and is consistent with the evaluations on thoracic CT and 3D-DSA datasets. Note that the values of AUC and MedNR do not change with the change of evaluation methodology.

²HRF image database website: https://www5.cs.fau.de/research/data/fundus-images/

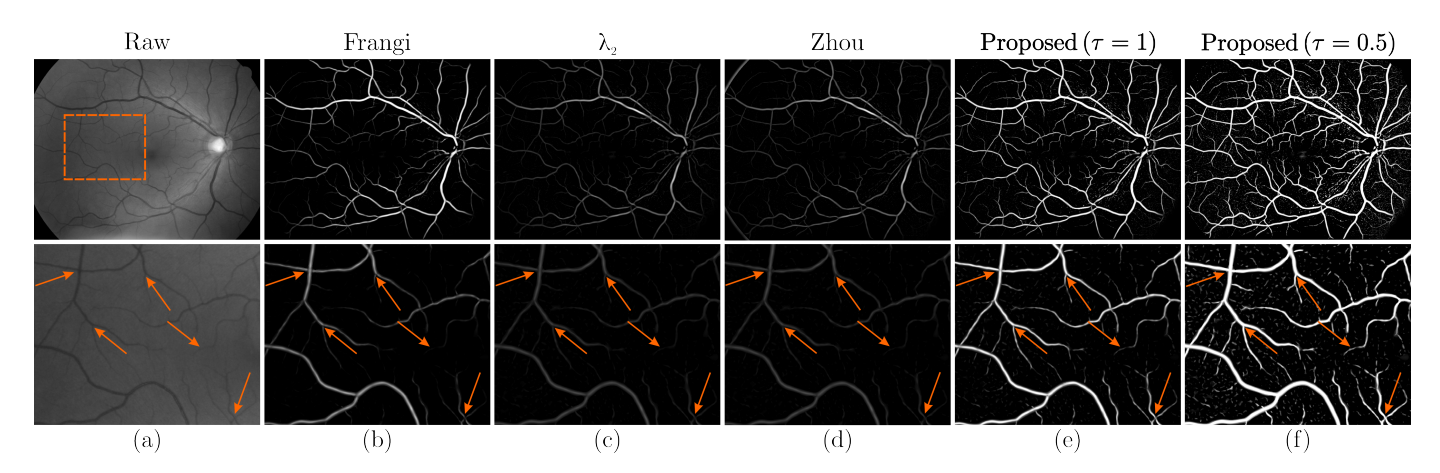


Fig. 6. Normalized grayscale image of 2D HRF color image [23] and the responses of multiscale filter with established and proposed enhancement functions. *Top row* shows a large field of view, while *bottom row* shows enlarged image region in *dashed square* of the raw image. *Arrows* indicate bifurcations and small vessels, in which established enhancement functions give a poor response.

Although a simple HRF segmentation based on multiscale filter responses cannot compete with the best segmentation result in terms of AUC, the obtained values of AUC>0.94 are very high. The slightly lower AUC in comparison to [23] is due to low contrast structures and artifacts in the background that are otherwise not connected to the fundus vasculature, but are anyway enhanced. Nevertheless, the obtained ACC and SP are higher for the proposed function. The mean AUC, ACC, SE, and SP of the multiscale filter based on the proposed enhancement function were comparable to other functions, while MedNR was substantially higher even at $\tau = 1$. Decreasing τ from 1 to 0.5 further increased the MedNR from 0.65 to 0.98. The impact of higher MedNR can be observed visually in the responses shown in Fig. 6. The main drawback of responses obtained by using Frangi's and, especially, λ_2 and Zhou's functions is that, compared to vessels with large diameters, the vessels with small diameters are poorly enhanced and thus poorly visible as illustrated by Fig. 6. Besides, even for the large-diameter vessels the response varies considerably, which is indicated by low MedNR values in Table IV. Conversely, the response based on the proposed function has uniform intensity on small and large diameter vessels and thus allows clear visualizations of large as well as small vessels. On the other hand, the high uniformity of the proposed filter results in the enhancement of some background image artifacts, the prominence of which increases with decreasing value of τ . Nevertheless, the use of additional simple morphological postprocessing methods can effectively eliminate these artifacts while retaining the enhanced vasculature.

Important differences between the multiscale responses of the proposed versus other enhancement functions can be observed at bifurcations, some of which are marked with arrows in Fig. 6. The other functions generally yielded low responses at bifurcations. In several cases the response disconnected the branching vessels from the main vessel. This can adversely affect a subsequent segmentation algorithm that relies on the enhancement of vascular structures [35], [36]. The filter responses based on the proposed function well preserved vessel connectivity at bifurcations.

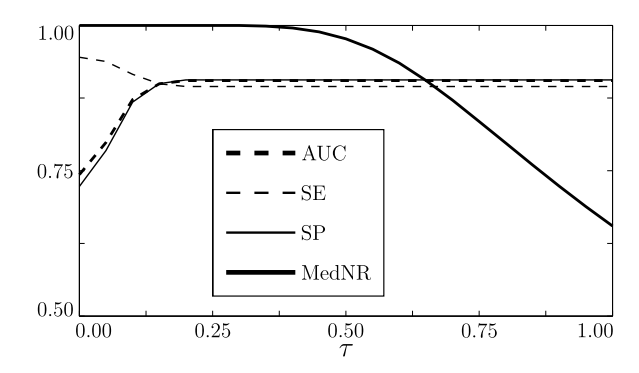


Fig. 7. Mean values of AUC, SE, SP and MedNR metrics, computed for the responses of multiscale filter with the proposed enhancement function, over 45 HRF color images shown with respect to parameter τ (13).

Similarly as for the 3D-DSA images, the regularization parameter τ of the proposed enhancement function was varied from 0 to 1 and, based on the responses on 45 HRF images, the mean AUC, SE, SP and MedNR were computed. The corresponding plots are shown in Fig. 7, which closely resemble the plots in Fig. 4 for the 3D-DSA images. On 2D fundus images the parameter τ had the same impact on evaluation metrics as on 3D-DSA images.

D. Visual Evaluation on Clinical Images

To further demonstrate the performance and wide applicability of the proposed enhancement function, we applied it to 3D TOF-MRA and contrast enhanced 2D X-ray angiograms of cerebral vasculatures and to a 3D-DSA image containing an aneurysm. The widely used Frangi's enhancement function was also applied and together with raw images used in a comparative visual assessment.

In cerebral TOF-MRA the visual contrast of certain vascular structures may be adversely influenced by a signal from adjacent non-vascular structures, e.g. thin lateral vessels in temporal lobes near the skull are poorly visualized due to the MR signal from dura matter, fat, skin, etc. (Fig. 8). Hence, visual assessment of these vessels can be difficult. In such situations, an enhancement function like the proposed can

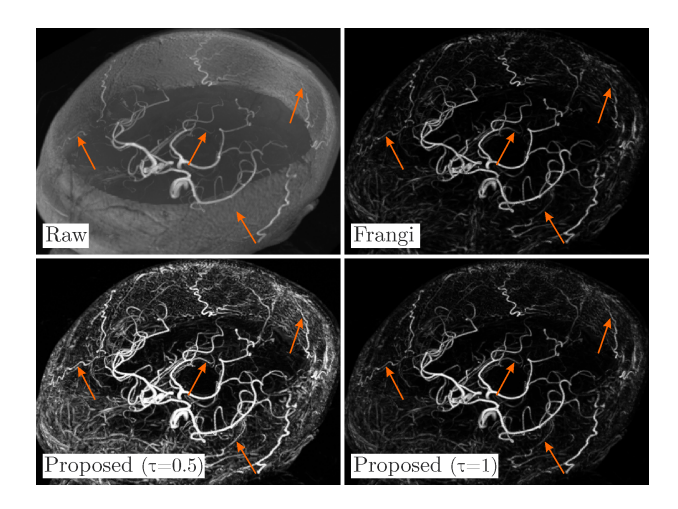


Fig. 8. Maximum intensity projections of cerebral TOF-MRA and corresponding responses of Frangi's and the proposed ($\tau=1$ and $\tau=0.5$) enhancement functions. Arrows indicate thin vessels with low visual contrast in TOF-MRA.

be applied to selectively enhance the vessels and suppress the non-vascular structures. Fig. 8 shows the TOF-MRA enhanced with the proposed and Frangi's enhancement functions. Compared to raw TOF-MRA, the enhanced images obviously suppress the signal adjacent to the skull and thereby better visualize the vessels close to the skull. The proposed function was run with $\tau=1$ and $\tau=0.5$, whereas the latter enhanced more non-vessel structures and artifacts in the background with the benefit of a more uniform enhancement of vessels at different anatomical sites. Compared to Frangi's, the proposed function better enhanced thin vessels (Fig. 8).

Contrast enhanced 2D X-ray angiography is widely used for the detection and assessment of vascular pathologies, and as live feedback for navigation during treatment. For these purposes a good visual contrast of vascular structures is important, but, unfortunately, it is often not obtained at distant vessels because of dissolution and reduced flow of the contrast agent. Fig. 9 shows a contrast enhanced X-ray of cerebral vasculature, in which thin vessels are poorly visible (indicated by the arrows). The Frangi's function did not enhance the poorly contrasted thin vessels. On the other hand, the proposed function enhances most of the distant thin vessels, some of which are barely seen in the raw X-ray image. Tuning parameter τ of the proposed function presents a trade-off between undesired enhancement of non-vascular structures and the uniformity of vascular structures' enhancement.

Enhancement of vascular pathologies is important for their detection and assessment. Fig. 10 shows an example of aneurysm enhancement by original and modified Frangi's and the proposed ($\tau=1$ and $\tau=0.5$) functions. The modified Frangi's function (4) does not contain the blob suppression term and thus has a higher intensity and a more uniform response within the aneurysm compared to the original function. Nevertheless, compared to the proposed function, the modified Frangi's function shows considerable intensity variations within the aneurysm, which are also visible in the raw image. Conversely, the proposed function effectively suppressed these variations and yielded high intensity and

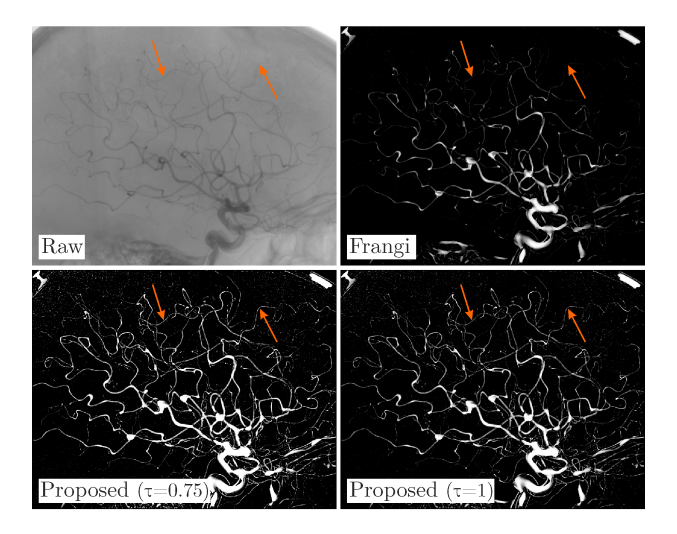


Fig. 9. Cerebral 2D X-ray and corresponding response of Frangi's and proposed ($\tau=1$ and $\tau=0.75$) enhancement function. Arrows indicate poorly contrasted distant vessels.

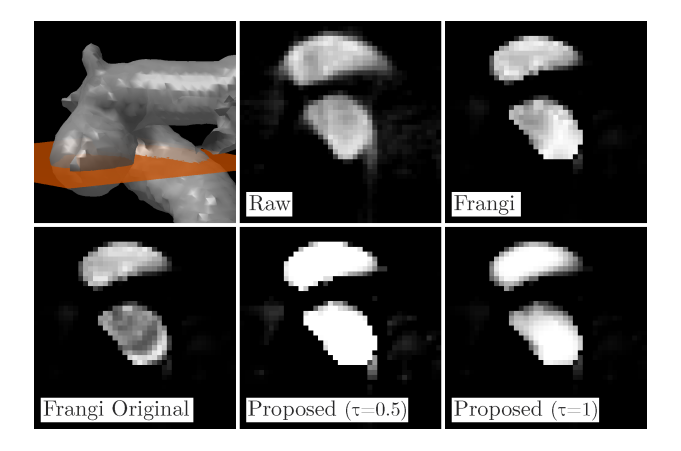


Fig. 10. Aneurysm and its parent vessel extracted from cerebral 3D-DSA and visualized in 3D, medial aneurysm cross-section of the raw 3D-DSA and corresponding responses of modified Frangi's, original Frangi's and the proposed ($\tau=1$ and $\tau=0.5$) enhancement functions.

highly uniform response.

V. DISCUSSION AND CONCLUSION

Multiscale Hessian based filtering is often used to enhance angiographic images for the purpose of computer-aided detection of vascular pathologies [7] and to improve 3D visualization [11] or segmentation of vascular structures [9]. However, established enhancement functions applied in the multiscale filter generally produce a rather poor and nonuniform response for natural variations of vascular morphology (different vessel diameters, spherical-elliptical crosssections), at bifurcations and aneurysms, etc. (Fig. 1). Such a deficient response will likely have an adverse impact on subsequent analysis of the enhanced images. For instance, no or weak response at a bifurcation may disrupt vessel lumen segmentation [9]. In this paper we therefore make three important contributions: i) review established 3D and 2D enhancement functions and elaborate their deficiencies, ii) propose a novel enhancement function, which overcomes these deficiencies and iii) quantitatively and qualitatively evaluate

and compare several established and the novel enhancement function on clinical image datasets of the lung, cerebral and fundus vasculatures.

The main reason for a rather poor and non-uniform enhancement obtained at certain structures by the established functions is that their response is proportional to the magnitudes of Hessian eigenvalues (λ_2 in Fig. 1), which in turn are proportional to intensities of the image to be enhanced. Hence, structures with undesired intensity variations in the original image will also manifest these undesired variations in the enhanced image. This may be a problem in angiographic images of larger vascular networks, in which substantial intensity variations are often observed as a result of varying vessel morphology, blood flow characteristics and/or contrast agent distribution. Another deficiency is the suppression of rounded structures, which adversely impacts the response at bifurcations and vessel aneurysms (responses marked with † in Fig. 1). Although we modified the original expressions such that they also enhance rounded structures, the responses were still rather poor at bifurcations and aneurysms. This is linked to another important deficiency in the design of established functions, which is their sensitivity to non-circular cross-sections of the structures. For instance, at bifurcations the vessel cross-section expands unilaterally from circular $(\lambda_2 \approx \lambda_3)$ to non-circular $(|\lambda_2| < |\lambda_3|)$, thus the functions (4– 8) that indicate relations $\lambda_2 \approx \lambda_3 \wedge |\lambda_{2,3}| \gg 0$ yield a lower response. Finally, most established functions were designed to enhance 3D images. To be applicable to 2D images these functions need to be modified, however, the expressions and characteristics of the original functions may not be preserved.

The novel enhancement function proposed in (15) was designed to indicate the eigenvalue relations $0 < \lambda_3/\lambda_2 \le 2$, thereby accounting for structures with elliptic cross-sections with the ratio of minor and major semi axes from 1:1 to 1:2. Inspired by volume ratio [32] the function design was advanced to enhance elongated and rounded structures. The main benefit of the ratio of eigenvalue magnitudes is that it effectively cancels the magnitude decays towards a structure's periphery. It also normalizes the response across different scales and thus exhibits a similar response on structures of different sizes. In image regions of uniform intensity, however, all eigenvalue magnitudes are low and the ratio is illbehaved. This problem has been addressed by regularizing the eigenvalue with the highest λ_3 magnitude to a fraction τ of the overall highest λ_3 magnitude. Although the proposed function was developed for enhancing 3D images, the same expression can be used to enhance 2D images by introducing an auxiliary eigenvalue λ_3 using (??). This is a unique feature of the novel function when compared to the established functions. The main benefit of this feature is that the novel function behaves similarly in 3D and 2D.

Thresholding thoracic CTs enhanced with the proposed function yielded a good segmentation of lung vasculature according to high AUC, which was the second best. The best performing method according to AUC (UofA_vision) was based on feature learning and classification and was far more complex. An important requirement of this method is to have a large image dataset with accurate, reliable and representative

reference annotations for learning discriminative features and training the classifier. For this purpose three training lung CT datasets were used. Because the same expert rater(s) chose the landmarks at specific locations in both the training and test datasets, the classifier was probably sensitive to the specific locations of landmarks, which might have biased the final results. On the contrary, training datasets are not required for segmentation based on the multiscale Hessian-based filter. Furthermore, the filter based on the proposed function had the highest SE and SP (0.962 and 0.961, respectively) among all tested methods.

The landmark based evaluation strategy used in VESSEL12 grand challenge dataset has certain limitations. According to the authors [25], negative landmarks tend to be located several pixels from the real vessel border, thus not penalizing oversegmentation close to vessel borders, nor segmentations in noisy areas where vessels are obviously not to be found. Another strategy could be to create a high quality segmentation of a complete 3D vasculature, which would allow for as many positive and negative landmarks as desired, however, on clinical images this is extremely difficult, subjective and time consuming to perform. We compared the two evaluation strategies (see Supplemental material) on synthetic datasets and found that both yield identical ranking of the methods. Since we wanted to keep the evaluation strategy consistent across different datasets, the experiments on cerebral 3D-DSAs used the landmark based evaluation strategy with 250 positive landmarks placed on vascular structures and 250 negative landmarks placed in the vicinity of the vessels (Fig. 3).

Results on the cerebral 3D-DSA dataset and the 2D fundus images showed that Hessian filtering with the proposed enhancement function achieved the highest AUC and MedNR among all tested functions, thus showing good segmentation performance and highly uniform enhancement of all vascular structures. The impact of (non)uniform enhancement is clearly seen on maximum intensity projections of the filter responses in Fig. 5. The proposed function better enhanced the vasculature, as indicated by the reduced intensity variations within the large internal carotid artery, clearly visible aneurysm and several of smaller vessels. The fundus images in Fig. 6 enhanced by the established functions show several vessels disconnected at bifurcations and crossings, which is not the case for the response of the proposed function. Furthemore, the proposed function enhanced the retinal vasculature more uniformly, especially for $\tau = 0.5$, visualizing several smaller vessels.

Sizes of vascular structures may vary substantially in angiographic images of large vascular networks, therefore, choosing a wide range of scales is crucial to enhance all the structures in the network. This may increase the computational demand of Hessian based filters, since for each scale a convolution of the image with correspondingly scaled Gaussian has to be performed to obtain the Hessian matrices. Then, for each scale, the eigenvalue decompositions of 3×3 or 2×2 Hessian matrices are computed with the analytical method [30] and the enhancement functions evaluated. To speed up the multiscale Hessian filter we performed all computations on an NVidia 450GTS GPU. On 3D-DSAs of size $200\times200\times200$ the mean

computational times obtained over five scales were around 857 and 1048 ms for the established and the proposed enhancement functions, respectively. Compared to the established functions, which require one image pass, the proposed function requires two image passes, the first for regularization in (13) and the second for response in (15). Although the mean computational time increased by 22%, the enhancement based on the proposed function is still computed in roughly one second for a moderately sized image. This should not represent a bottleneck in image analysis framework for computer-aided detection [7] or vessel lumen segmentation [9], nor in 3D visualization [11] where the enhancement is executed only once before the visualization starts. Vascular structures usually represent less than 5% of voxels in a 3D image, thus if faster execution is required, a substantial speedup is possible by evaluating the multiscale Hessian filter (2) only in voxels, for which $\lambda_{1,2,3} < 0$ (dark on bright) or $\lambda_{1,2,3} > 0$ (bright on dark). Recently, Yang and Cheng [37] proposed a simple method to identify such voxels based on the elements of Hessian matrix, which in general reduced the computational times by 55% for 3D and 7.5% for 2D images.

In conclusion, we proposed a novel enhancement function for the popular multiscale Hessian based filter. Quantitative and visual evaluations on five clinical datasets showed that, compared to established functions, the proposed enhancement function yields good segmentation performance according to high AUC, SE and SP, and has a higher and more uniform response across all vascular structures. Because the observed enhancement is close to the one expected of an ideal enhancement function, the use of the proposed function on angiographic images has a large potential to simplify and significantly improve subsequent image analysis methods and visualizations.

ACKNOWLEDGMENT

This research was supported by the Slovenian Research Agency under grants L2-5472, J2-5473, and J7-6781.

REFERENCES

- [1] J. P. Villablanca, R. Jahan et al., "Detection and characterization of very small cerebral aneurysms by using 2D and 3D helical CT angiography," Am. J. Neuroradiol., vol. 23, no. 7, pp. 1187–1198, 2002.
- [2] W. van Rooij, M. Sprengers, A. de Gast, J. Peluso, and M. Sluzewski, "3d rotational angiography: The new gold standard in the detection of additional intracranial aneurysms," *Am. J. Neuroradiol.*, vol. 29, no. 5, pp. 976–979, 2008.
- [3] P. M. White, J. M. Wardlaw, and V. Easton, "Can noninvasive imaging accurately depict intracranial aneurysms? a systematic review," *Radiology*, vol. 217, no. 2, pp. 361–370, 2000.
- [4] A. M. H. Sailer, J. P. Grutters, J. E. Wildberger, P. A. Hofman, J. T. Wilmink, and W. H. van Zwam, "Cost-effectiveness of CTA, MRA and DSA in patients with non-traumatic subarachnoid haemorrhage," *Insights Imaging*, vol. 4, no. 4, pp. 499–507, 2013.
- [5] M. Abramoff, M. Garvin, and M. Sonka, "Retinal imaging and image analysis," *IEEE Rev. Biomed. Eng.*, vol. 3, pp. 169–208, 2010.
- [6] R. Shahzad, H. Kirili, C. Metz, H. Tang, M. Schaap, L. v. Vliet, W. Niessen, and T. v. Walsum, "Automatic segmentation, detection and quantification of coronary artery stenoses on CTA," *Int. J. Cardiovasc. Imaging*, vol. 29, no. 8, pp. 1847–1859, 2013.
- [7] C. M. Hentschke, O. Beuing, H. Paukisch, C. Scherlach, M. Skalej, and K. D. Tnnies, "A system to detect cerebral aneurysms in multimodality angiographic data sets," *Med. Phys.*, vol. 41, no. 9, p. 091904, 2014.

- [8] T. Jerman, F. Pernuš, B. Likar, and Z. Špiclin, "Blob Enhancement and Visualization for Improved Intracranial Aneurysm Detection," *IEEE Transactions on Visualization and Computer Graphics*, vol. In Press, 2015.
- [9] D. Lesage, E. D. Angelini, I. Bloch, and G. Funka-Lea, "A review of 3D vessel lumen segmentation techniques: Models, features and extraction schemes," *Med. Image Anal.*, vol. 13, no. 6, 2009.
- [10] G. Agam, I. Armato, S.G., and C. Wu, "Vessel tree reconstruction in thoracic CT scans with application to nodule detection," *IEEE Trans. Med. Imag.*, vol. 24, no. 4, pp. 486–499, 2005.
- [11] R. Wiemker, T. Klinder, M. Bergtholdt, K. Meetz, I. C. Carlsen, and T. Buelow, "A radial structure tensor and its use for shape-encoding medical visualization of tubular and nodular structures," *IEEE Trans. Vis. Comput. Graph.*, vol. 19, no. 3, pp. 353–366, 2013.
- [12] K. Krissian, G. Malandain, N. Ayache, R. Vaillant, and Y. Trousset, "Model-based detection of tubular structures in 3D images," *Comput. Vision Image Understanding*, vol. 80, no. 2, pp. 130–171, 2000.
- [13] A. F. Frangi, W. J. Niessen, K. L. Vincken, and M. A. Viergever, "Multiscale vessel enhancement filtering," in *Medical Image Computing and Computer-Assisted Intervention - MICCAI'98*, W. M. Wells, A. Colchester, and S. Delp, Eds. Berlin: Springer-Verlag Berlin, 1998, vol. 1496, pp. 130–137.
- [14] Y. Sato, C. F. Westin, A. Bhalerao, S. Nakajima, N. Shiraga, S. Tamura, and R. Kikinis, "Tissue classification based on 3D local intensity structures for volume rendering," *IEEE T. Vis. Comput. Gr.*, vol. 6, no. 2, pp. 160–180, 2000.
- [15] Q. Li, S. Sone, and K. Doi, "Selective enhancement filters for nodules, vessels, and airway walls in two- and three-dimensional CT scans," *Med. Phys.*, vol. 30, no. 8, pp. 2040–2051, 2003.
- [16] M. Erdt, M. Raspe, and M. Suehling, "Automatic Hepatic Vessel Segmentation Using Graphics Hardware," in *Proc. of the 4th International Workshop on Medical Imaging and Augmented Reality*, ser. MIAR '08. Berlin, Heidelberg: Springer-Verlag, 2008, pp. 403–412.
- [17] C. Zhou, H.-P. Chan, B. Sahiner, L. M. Hadjiiski, A. Chughtai, S. Patel, J. Wei, J. Ge, P. N. Cascade, and E. A. Kazerooni, "Automatic multiscale enhancement and segmentation of pulmonary vessels in CT pulmonary angiography images for CAD applications," *Med. Phys.*, vol. 34, no. 12, pp. 4567–4577, 2007.
- [18] M. Jiang, Q. Ji, and B. McEwen, "Model-Based Automated Extraction of Microtubules From Electron Tomography Volume," *IEEE T. Inf. Technol.* B., vol. 10, no. 3, pp. 608–617, 2006.
- [19] R. Manniesing, M. A. Viergever, and W. J. Niessen, "Vessel enhancing diffusion - A scale space representation of vessel structures," *Med. Image Anal.*, vol. 10, no. 6, pp. 815–825, 2006.
- [20] C. Bauer and H. Bischof, "A Novel Approach for Detection of Tubular Objects and Its Application to Medical Image Analysis," in *Pattern Recognition*, ser. Lecture Notes in Computer Science, G. Rigoll, Ed. Springer Berlin Heidelberg, 2008, no. 5096, pp. 163–172.
- [21] M. W. K. Law and A. C. S. Chung, "An Oriented Flux Symmetry Based Active Contour Model for Three Dimensional Vessel Segmentation," in Computer Vision ECCV 2010, ser. Lecture Notes in Computer Science, K. Daniilidis, P. Maragos, and N. Paragios, Eds. Springer Berlin Heidelberg, 2010, no. 6313, pp. 720–734.
- [22] B. Zhang, L. Zhang, L. Zhang, and F. Karray, "Retinal vessel extraction by matched filter with first-order derivative of Gaussian," *Comput. Biol. Med.*, vol. 40, no. 4, pp. 438–445, 2010.
- [23] J. Odstrcilik, R. Kolar, A. Budai, J. Hornegger, J. Jan, J. Gazarek, T. Kubena, P. Cernosek, O. Svoboda, and E. Angelopoulou, "Retinal vessel segmentation by improved matched filtering: evaluation on a new high-resolution fundus image database," *IET Image Process.*, vol. 7, no. 4, pp. 373–383, 2013.
- [24] H. M. Luu, C. Klink, A. Moelker, W. Niessen, and T. van Walsum, "Quantitative evaluation of noise reduction and vesselness filters for liver vessel segmentation on abdominal CTA images," *Physics in Medicine* and Biology, vol. 60, no. 10, pp. 3905–3926, 2015.
- [25] R. D. Rudyanto, S. Kerkstra et al., "Comparing algorithms for automated vessel segmentation in computed tomography scans of the lung: the VESSEL12 study," Med. Image Anal., vol. 18, no. 7, pp. 1217–1232, 2014.
- [26] A. Goyal, J. Lee, P. Lamata, J. van den Wijngaard, P. van Horssen, J. Spaan, M. Siebes, V. Grau, and N. Smith, "Model-based vasculature extraction from optical fluorescence cryomicrotome images," vol. 32, no. 1, pp. 56–72, 2013.
- [27] N. Baka, C. Metz, C. Schultz, R.-J. van Geuns, W. Niessen, and T. van Walsum, "Oriented gaussian mixture models for nonrigid 2D/3D coronary artery registration," *IEEE Trans. Med. Imag.*, vol. 33, no. 5, pp. 1023–1034, 2014.

- [28] W. Zhang, J. Liu, J. Yao, A. Louie, T. Nguyen, S. Wank, W. Nowinski, and R. Summers, "Mesenteric vasculature-guided small bowel segmentation on 3-D CT," *IEEE Trans. Med. Imag.*, vol. 32, no. 11, pp. 2006–2021, 2013.
- [29] T. Jerman, F. Pernuš, B. Likar, and Z. Špiclin, "Beyond Frangi: an improved multiscale vesselness filter," in *Proc. SPIE Medical Imaging* 2015: Image Processing, vol. 9413, 2015, pp. 94132A–11.
- [30] J. Kopp, "Efficient numerical diagonalization of Hermitian 3x3 matrices," Int. J. Mod. Phys. C, vol. 19, no. 03, pp. 523–548, 2008.
- [31] T. H. J. M. Peeters, P. R. Rodrigues, A. Vilanova, and B. M. t. H. Romeny, "Analysis of distance/similarity measures for diffusion tensor imaging," in *Visualization and Processing of Tensor Fields*, ser. Mathematics and Visualization, D. Laidlaw and J. Weickert, Eds. Springer Berlin Heidelberg, 2009, pp. 113–136.
- [32] C. Pierpaoli and P. J. Basser, "Toward a quantitative assessment of diffusion anisotropy," *Magn. Reson. Med.*, vol. 36, no. 6, pp. 893–906, 1996.
- [33] T. Fawcett, "An introduction to ROC analysis," *Pattern Recogn. Lett.*, vol. 27, no. 8, pp. 861–874, 2006.
- [34] R. Kiros, K. Popuri, D. Cobzas, and M. Jagersand, "Stacked multiscale feature learning for domain independent medical image segmentation," in *Machine Learning in Medical Imaging*, ser. Lecture Notes in Computer Science, G. Wu, D. Zhang, and L. Zhou, Eds. Springer International Publishing, 2014, no. 8679, pp. 25–32.
- [35] M. M. Fraz, P. Remagnino, A. Hoppe, B. Uyyanonvara, A. R. Rudnicka, C. G. Owen, and S. A. Barman, "Blood vessel segmentation methodologies in retinal images a survey," *Comput. Meth. Prog. Bio.*, vol. 108, no. 1, pp. 407–433, 2012.
- [36] E. Cheng, L. Du, Y. Wu, Y. J. Zhu, V. Megalooikonomou, and H. Ling, "Discriminative vessel segmentation in retinal images by fusing contextaware hybrid features," *Mach. Vision Appl.*, vol. 25, no. 7, pp. 1779– 1792, 2014.
- [37] S.-F. Yang and C.-H. Cheng, "Fast computation of Hessian-based enhancement filters for medical images," *Comput. Meth. Prog. Bio.*, vol. 116, no. 3, pp. 215–225, 2014.